Article

Robustness of a Steel Truss Bridge Subjected to Sudden Member Breakage during the Continuous-to-Simply-Supported Transition

Yanming Chen [1], Yong Liao [2], Liming Zhu [1,*] , Lingkun Chen [3] and Yilian Chen [1]

[1]   College of Transportation Engineering, Nanjing Tech University, Nanjing 214000, China; ymchen@njtech.edu.cn (Yanming Chen)
[2]   China Railway No. 2 Engineering Group Co., Ltd., Chengdu 610031, China
[3]   College of Architecture Science and Engineering, Yangzhou University, Yangzhou 225000, China
[*]   Correspondence: zhulm@njtech.edu.cn

Abstract: Steel truss bridges are especially vulnerable in the event of a sudden loss of a load-carrying element, which can trigger a chain of failures. This paper describes a unique case study of a steel truss bridge under construction subjected to sudden member breakages with an extensive monitoring system. The failures occurred during the dismantlement of temporary members that had been used to transform a three-span simply supported steel truss bridge into a three-span continuous structure during incremental launching. These temporary members needed to be removed once the bridge reached its final position. The robustness of the bridge was assessed using computer simulations of various failure scenarios to evaluate its capacity to effectively activate alternative load paths (ALPs). The results demonstrated the structural redundancy of the steel truss bridge. However, the dynamic response resulting from the failure of the temporary upper chord, due to the initially high tension in the rods, should not be overlooked. To mitigate this issue, a structural retrofitting method was proposed, involving jacking the truss girder above the side pier to reduce the tension in the temporary upper chord above the middle pier. The effectiveness of this method was demonstrated through both simulated and formal experimental tests.

Keywords: failure; robustness; robustness-enhanced method; steel truss bridge; sudden member breakage

1. Introduction

Steel truss bridges became widely used structures due to their simplicity and load-carrying efficiency. However, steel truss bridges are especially vulnerable in the event of a sudden loss of a load-carrying element, in which the bridge immediately experiences an alteration of its load paths, developing progressive collapse [1–3]. For example, the Skagit River bridge (2013) collapsed due to a truck impact and drag of one sway frame member [4]; the Chauras bridge (2012) collapsed after buckling of top chord compression members [5]; the I-35 W Mississippi truss bridge (2007) collapsed due to the fracture of undersized gusset plates; the Seongsu bridge (1994) collapsed due to an undetected crack propagation and the subsequent failure of a key connection; and the Quebec bridge (1907) collapsed due to the failure of one of its chords [6]. A study conducted in the US [7] identified more than 500 steel truss-type bridge failures in a period of 11 years (1989–2000). Several causes for these failures exist, including fatigue, overloading, corrosion, and collisions [8,9].

An initial local failure in a structural component of a steel truss bridge can commonly lead to a rapid chain reaction of subsequent failures within a short period [10,11]. The effects of initial local failure have raised the interest of many researchers, and collapse databases have been created, providing valuable insights for preventing such failures [12–14]. Russell reviewed robustness considerations in Eurocodes and other international codes [15]. Adam conducted a comprehensive review of the major advancements made in the 21st century

with regards to progressive collapse [16]. Santiago López collected information from 25 case studies to build a novel database of detailed information on the initial damage and its propagation, as well as the consequences of the collapse. The results allowed the identification of the most frequent initial constituted damage states or failures leading to progressive collapse [3]. Patricia Vanova assessed the dynamic responses of a bridge under random excitation, in which damage scenarios with various crack locations and severities were considered for a member [17]. Several scaled models were built to study structural robustness and more realistic structural responses [18]. Padil et al. built a scaled model of a steel truss bridge in a laboratory, where they simulated three damage scenarios by cutting specific members using several cuts [19]. Teng et al. studied both a scaled laboratory model and a real steel truss bridge by testing the acceleration signals of the physical bridge considering five structural scenarios [20]. Buitrago and Bertolesi examined a full-scale 21-metre bridge span, which was tested under laboratory conditions to provide practical recommendations for the early detection of local failures that could potentially lead to a progressive collapse [21,22]. Caredda examined the structure's capacity to activate alternative load paths, and then noted that continuous structural monitoring is also recommended with the optimal arrangement of sensors to be able to predict in time the occurrence of local failures and prevent the complete failure of the entire structure [23].

This paper describes the research team's unique opportunity to study a full-scale steel truss bridge with the aims of (1) simulating and experimentally analyzing its robustness, (2) evaluating the performance of an unconventional continuous-to-simply-supported incremental launching method, and (3) testing the effectiveness of the proposed structural retrofitting method for robustness enhancement. This study is novel and permitted an advance in two areas, namely, (i) an innovative incremental launching method for a steel truss bridge, and (ii) the analysis and experimental testing of the robustness in a steel truss bridge retrofitted with a robustness-enhanced method subjected to sudden member breakages.

To comply with these aims, after the Introduction, Section 2 presents a description of the real case used to carry out the continuous-to-simply-supported incremental launching method. Section 3 describes the computational simulation together with a description of the finite element (FE) model, the loads considered, and the verification process. Section 4 contains the main results of the robustness tests of the steel truss bridge subjected to sudden temporary member breakages. Section 5 contains a discussion of the structural retrofitting method for robustness enhancement obtained with simulated and formal experimental testing. Finally, Section 6 provides a summary of the conclusions.

2. Unconventional Incremental Launching Method

The incremental launching method has the characteristics of large span capacity, high safety, and strong applicability, and it is increasingly used in long-span bridges, especially steel bridges [24]. There are many application cases in long-span simply supported steel truss bridges [25,26]. The Yuyao River Bridge begins at the south of Zhuangqiao Station and the north of Lijiang West Road, crosses the Yuyao River, and ends on the south bank. The main bridge features a three-span simply supported steel truss girder with spans of 80 m + 128 m + 80 m across the Yuyao River. The panel length of the 128 m span is 16.0 m, and the truss height is 16.0 m. The panel length of the 80 m spans is 10.0 m, and the truss height is 11.6 m. The center-to-center distance between the two main trusses is 11.8 m. The main girder structure is constructed from Q370q and Q345q steel. Due to the limitations of the construction site conditions, including navigation and flood safety constraints, temporary piers cannot be added between the main piers. Consequently, conventional construction methods are inadequate. This project adopts an unconventional continuous-to-simply-supported incremental launching method for the first time. Temporary members are used to connect the three-span simply supported steel truss bridge, transforming it into a three-span continuous structure during incremental launching construction. These temporary members include temporary upper chords, horizontal connections, and lower chords. Temporary members are installed between the 128 m and 80 m spans on both the

north and south sides. Temporary upper chords and horizontal connections are assembled with adjacent node plates, while the temporary lower chords consist of two additional webs and one top plate added to the interior of the node plate at the end of the 128 m span, which are butt-welded to the 80 m span node plate on-site. After the bridge has been pushed to its design position, the temporary members are dismantled. The schematic diagram of the steel truss bridge is shown in Figure 1.
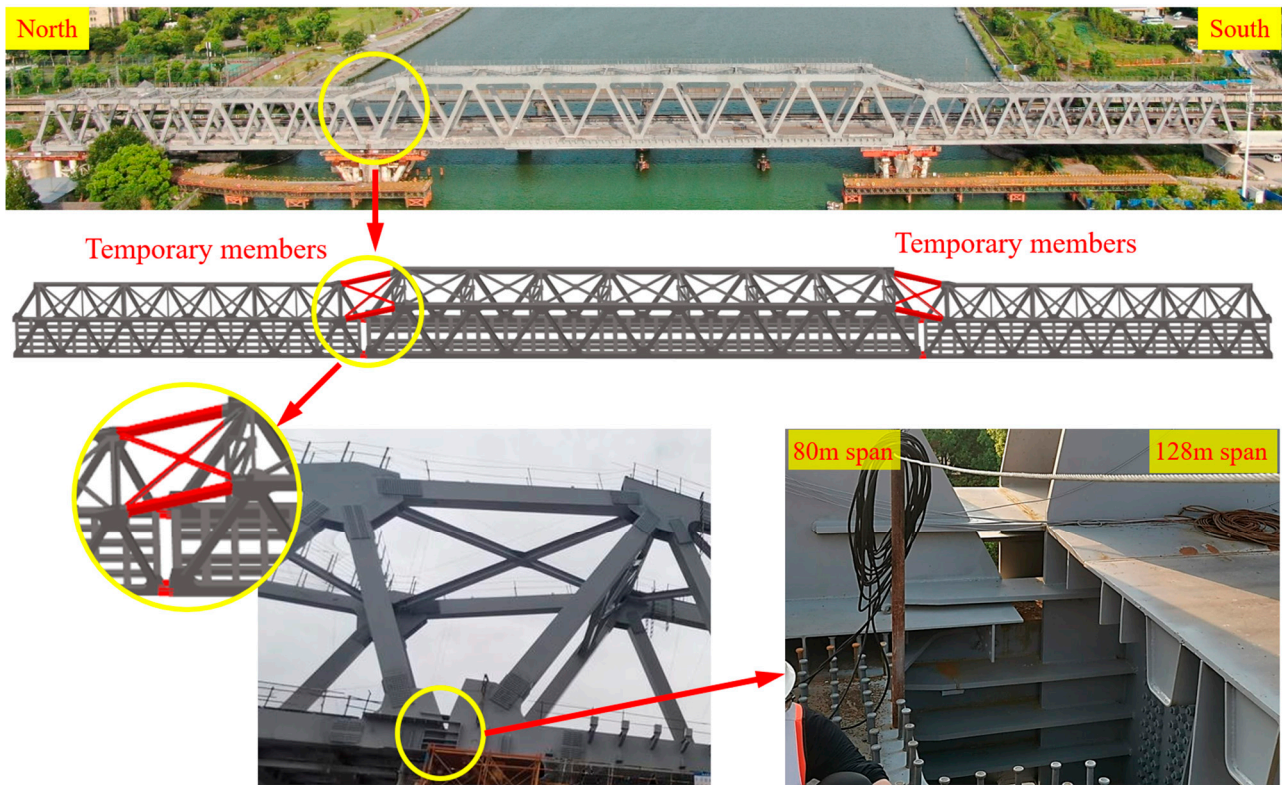

Figure 1. Schematic diagram of the steel truss bridge.

The incremental launching construction phase involves several key steps: assembling the steel truss girders in sections between temporary piers 10# and 12#, and using a cantilever assembly method for the entire process. The three-span simply supported steel truss girders are initially assembled into a three-span continuous configuration with the aid of temporary members. Subsequently, the steel truss girders are pushed forward over a significant distance. Incremental launching equipment is installed on the slipway girders of piers 11#, 12#, 13#, 14#, and 15#. Once the bridge reaches its design position, the temporary members are removed, converting the structure from a three-span continuous steel truss bridge to a three-span simply supported steel truss bridge. The detailed construction phases are outlined in Table 1.

Table 1. Continuous-to-simply-supported incremental launching construction phase.

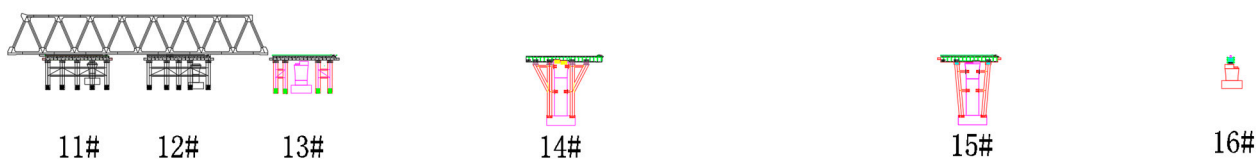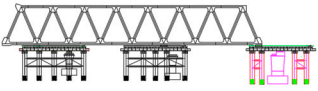Construction phase 1: assembling 80 m span steel truss girder
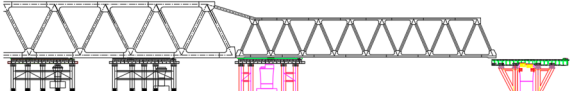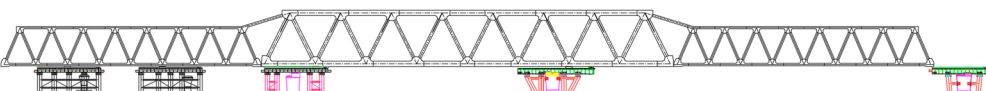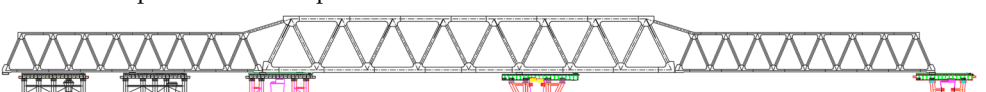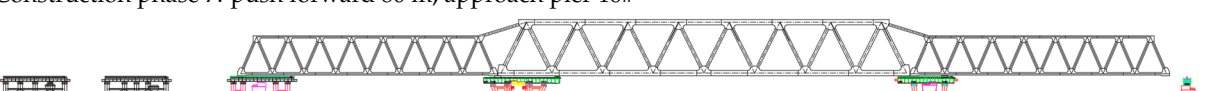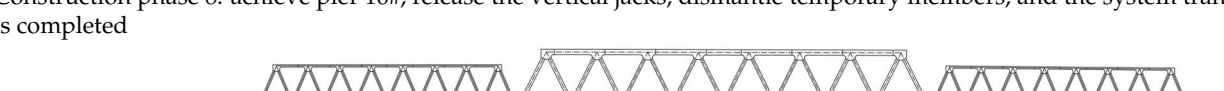
Table 1. *Cont.*

Construction phase 2: achieve pier 13#

11#　　12#　　13#　　　14#　　　　　　15#　　　　16#

Construction phase 3: push forward 80 m; the 4.5 span of 128 m steel truss girder assembly was completed

11#　　12#　　13#　　　14#　　　　　　15#　　　　16#

Construction phase 4: achieve pier 14#

11#　　12#　　13#　　　14#　　　　　　15#　　　　16#

Construction phase 5: push forward 128 m; the whole structure of steel truss bridge assembly was completed

11#　　12#　　13#　　　14#　　　　　　15#　　　　16#

Construction phase 6: achieve pier 15#

11#　　12#　　13#　　　14#　　　　　　15#　　　　16#

Construction phase 7: push forward 80 m, approach pier 16#

11#　　12#　　13#　　　14#　　　　　　15#　　　　16#

Construction phase 8: achieve pier 16#, release the vertical jacks, dismantle temporary members, and the system transformation is completed

11#　　12#　　13#　　　14#　　　　　　15#　　　　16#

3. Model and Verification

3.1. FEA Model

To analyze the structural response during the sudden failure of temporary members, a detailed finite element model of the entire bridge was created using ABAQUS 2022 software. This model employs shell elements (S4R) to represent all members and gusset plates, with a grid size ranging from 100 mm to 200 mm. The steel truss beam has a material density of 7.85 g/cm^3, an elastic modulus of 206 GPa, and a Poisson ratio of 0.3. Contact settings were defined as binding.

The finite element model utilizes a rectangular coordinate system where the X-axis represents the horizontal direction of the bridge, the Y-axis represents the vertical direction of the bridge, and the Z-axis represents the longitudinal direction of the bridge. Within this model, a reference point is established at the center of the contact area between the lower chord and the slider. This reference point is linked to the local region of the lower chord via "coupling" constraints. The reference point restricts translation in the Y-direction to simulate the slider support. Additionally, another reference point is positioned accordingly to constrain the displacement of the steel truss girder in both the transverse and longitudinal directions; this reference point restricts translation in the X- and Z-directions and rotation in the Y- and Z-directions. The construction stage loads primarily include the self-weight of the steel truss girders and the loads imposed by construction machinery. Since work on the girders is prohibited during the incremental launching construction process, live loads are not considered. The overall model utilizing refined shell elements is illustrated in Figure 2.
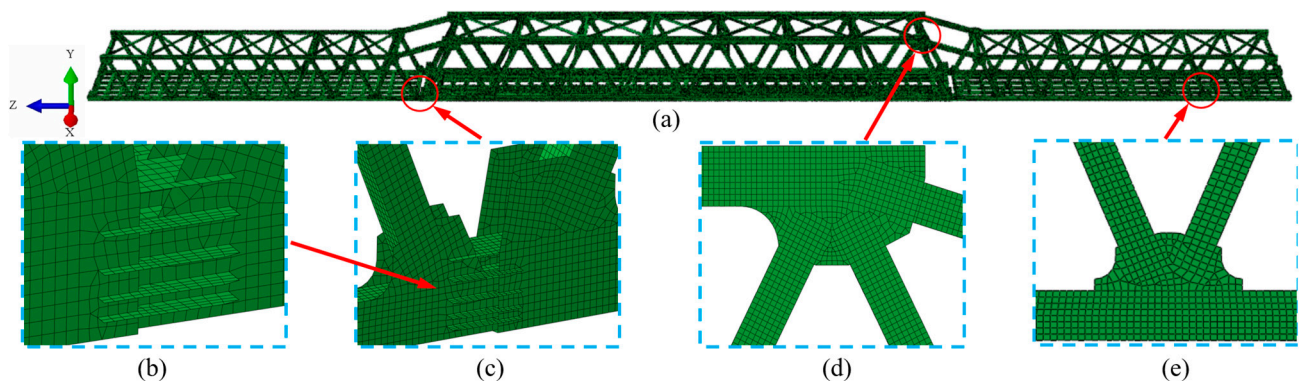
Figure 2. FEA model schematic diagram of steel truss bridge: (**a**) overall; (**b**) enlarged view of temporary lower chord; (**c**) temporary lower chord; (**d**) upper chord; (**e**) lower chord.

The quasi-dynamic simulation method, full-dynamic simulation method, and semi-dynamic simulation method are commonly employed to model the fracture of bars [27]. The accuracy of results across these three methods is generally comparable. In comparison to the quasi-dynamic and full-dynamic simulation methods, the semi-dynamic simulation method offers advantages such as reduced computational time and simpler implementation. Consequently, this paper employs the semi-dynamic simulation method to analyze the dynamic response of the entire structure after the temporary members have been severed. ABAQUS features the "life-and-death unit" technology, which allows for the simulation of member failure within a predefined time frame. The semi-dynamic simulation analysis is conducted as follows: First, the static internal forces of the members prior to fracture are determined through static analysis of the model. Subsequently, the members are severed using the "life-and-death unit", and a transient dynamic analysis is performed to assess the dynamic response of the structure to the sudden fracture of the members.

3.2. Measurement Arrangements

To ensure the safety of the steel truss bridge during incremental launching and system transformation construction, two types of measurements are collected during testing:

strains and displacements at key points previously identified from theoretical calculations. Strains are measured during the launching phase, converted to stresses, and compared with results obtained from finite element analysis.

A total of 19 measurement sections are selected for the upper chord, lower chord, web, and temporary members of the steel truss bridge. Measurement points are arranged for all sections on the east and west sides of the truss, with one section of each chord having measurement points on both the upper and lower edges. In total, 76 stress gauges are deployed, as shown in Figure 3. Vertical displacement at the front end of the main beam during the incremental launching process is also a crucial control index. The cantilever end of the bridge experiences vertical deformation due to the self-weight of the structure; therefore, a deformation monitoring point, specifically a prism, is established at the front end of the main girder and observed using a total station. During assembly, the elevation of the main girder before pushing is recorded as the initial value, with the measurement reference point set at the contact point between the front fulcrum pad and the bottom of the girder. The actual vertical deflection of the main girder is calculated as the difference between the bottom elevation of the beam at the front fulcrum and the cantilever end.
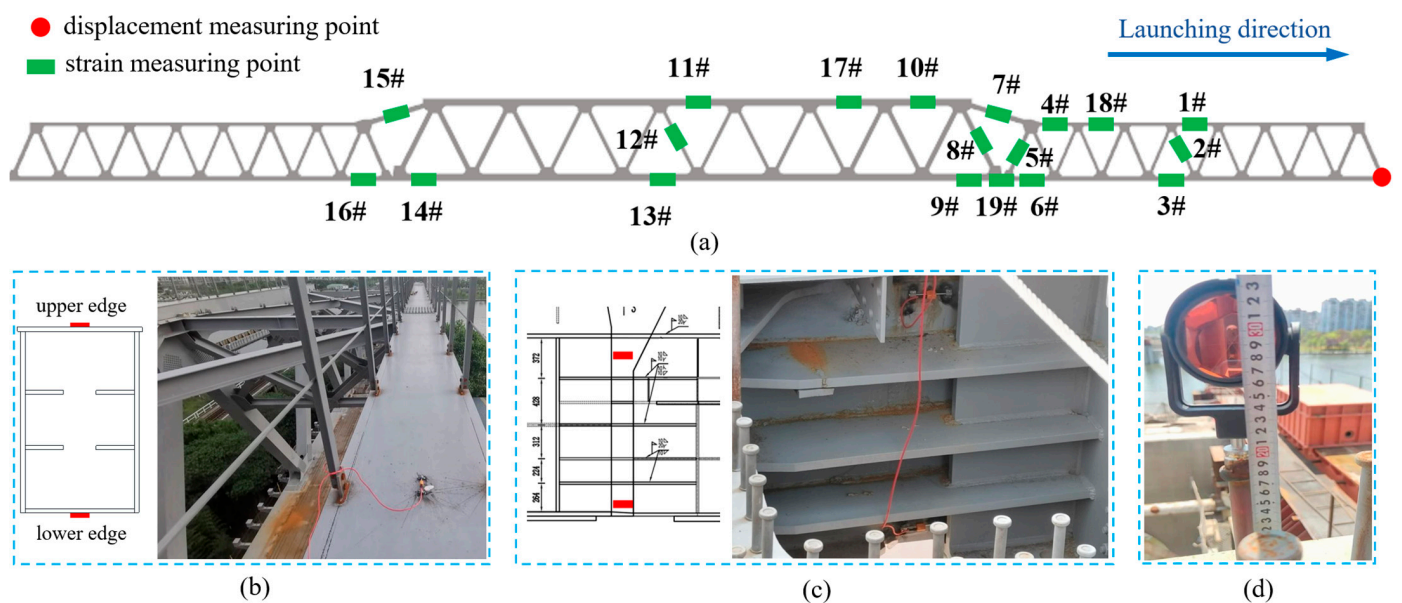
Figure 3. Layout of measuring points: (**a**) overall; (**b**) upper chord; (**c**) temporary lower chord; (**d**) displacement.

3.3. Verification

The comparison between the measured and calculated stress of the temporary upper chord (section 7#) is shown in Figure 4b, while the comparison between the measured and calculated vertical displacement at the front end is presented in Figure 4c. In these figures, positive values indicate uplift, and negative values represent downward deflection. Throughout the entire launching construction, the trends of the measured and calculated values are generally consistent. Just before the 15# pier, the main girder is in its maximum cantilever state, with the deflection of the front end reaching 922.70 mm, while the corresponding calculated value is 795.22 mm, resulting in a difference of 13.8%. The measured stresses at the upper and lower edges of the temporary upper chord are 101.4 MPa and 95.1 MPa, respectively, compared to calculated values of 96.5 MPa and 85.7 MPa, leading to differences of 6.2% and 11.2%. The differences between the measured and calculated stress values are mainly due to variations in the height of the bearing pads placed on the piers during the launching construction. Specifically, when the bridge front end reaches the pier, multiple steel bearing pads are stacked on top of the pier as temporary supports for the steel truss bridge. However, during the actual construction process, due to factors such as

uneven contact surfaces between the bearing pads and minor height differences in each pad, the total height of the steel bearing pads placed on each pier is not exactly uniform. In contrast, in the model calculations, the bearing pad height was considered to be consistent, leading to the observed differences between the measured and calculated stress values. Temporary supporting devices of the same specification can be used in subsequent similar cases, which can reduce the influence of this factor. Overall, the measured results verify the effectiveness of the ABAQUS model, which can be used as a reliable basis for the next research work.

(a) Deformation schematic diagram of FEM

(b) Stress of temporary upper chord

(c) Deformation of the main girder front end
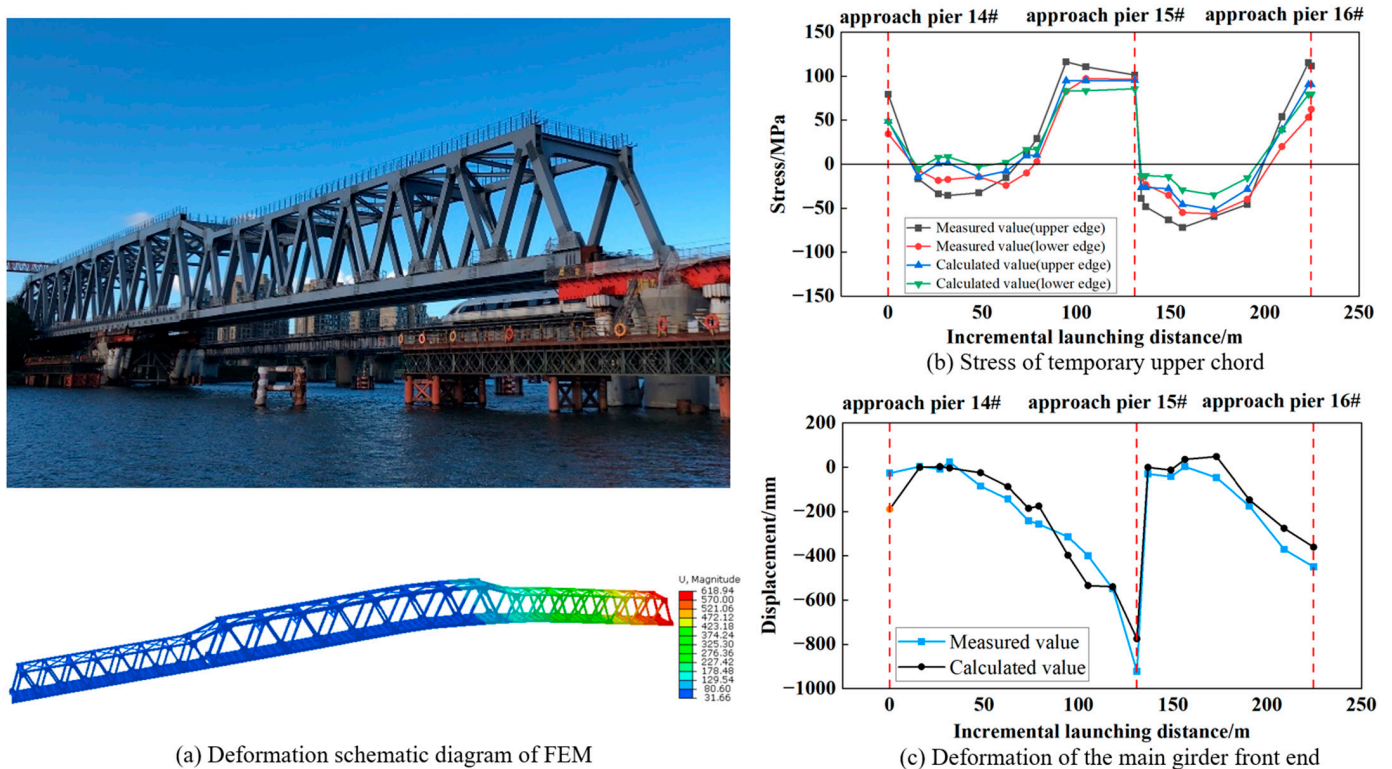
Figure 4. Calculated and measured results during incremental launching construction.

4. Robustness

This section examines failure scenarios of temporary members based on field engineering conditions. The robustness of the structure was evaluated through computer simulations of various damage scenarios to assess the bridge's ability to effectively activate alternative load paths. Additionally, dynamic response analyses were conducted for the specific failure scenarios identified.

4.1. Failure Scenarios

Unlike some studies where a designed sequence of structural damage is necessary to analyze behavior with the evolution of deliberately induced damage [21], the case described in this paper is constrained by construction methods and engineering principles. The breakage sequence must ensure the clarity of the bridge's structural system. Specifically, all temporary members on either the south or north side must be dismantled first, converting the three-span continuous bridge into a two-span continuous bridge and a single 80 m span simply supported bridge. Subsequently, all temporary members on the remaining side are removed to transform it into a three-span simply supported bridge. Figure 5 illustrates the failure scenarios associated with different dismantling steps. On one side, the temporary members fail in the sequence of horizontal connection, one upper chord, another upper chord, and finally the lower chord, followed by the same sequence of failure on the other side.
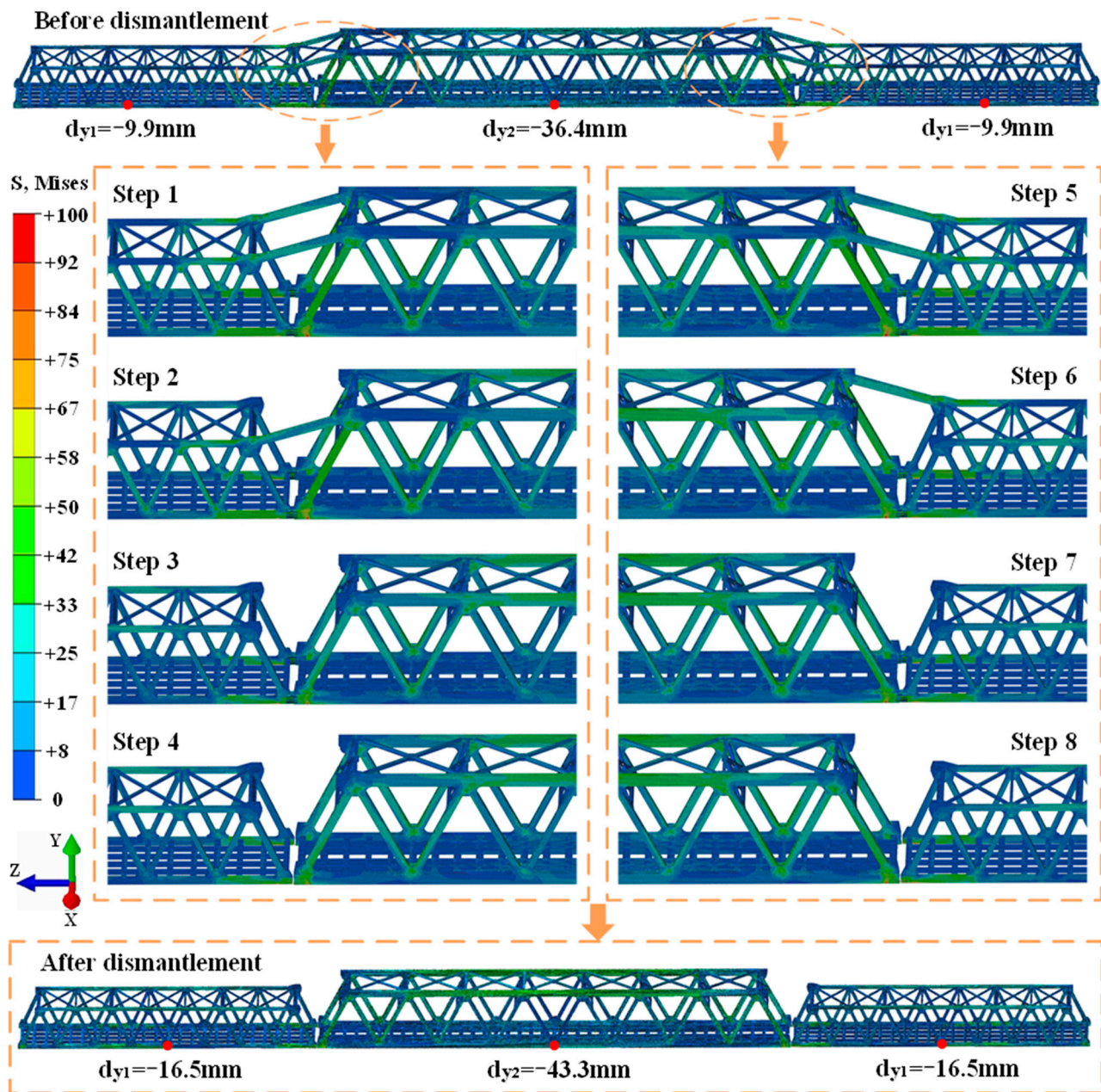
Figure 5. Von Mises stress for different failure scenarios. Units: Mpa.

4.2. Alternative Load Paths

The impact of dismantling temporary members on the overall structure is complex, as evidenced by the sudden and uncontrollable changes in stress redistribution [28,29]. Figure 5 illustrates the stress contour maps from FE analysis under various failure scenarios. The failure of temporary horizontal connections and lower chords has a minimal effect. In contrast, failures of temporary upper chords significantly affect the nearby upper chords and members in the midspan. Specifically, stresses in the upper chords near the failure site increased by up to 270%, rising from 5.61 MPa to 20.73 MPa. Stresses in the upper chords at the midspan increased by up to 43%, changing from 27.08 MPa to 38.65 MPa. Despite these stress increases, the structural stress remains within a safe range during the construction stage, as there are no vehicle loads. The diagram also indicates that the maximum deflection increased by up to 19.0% in the middle span and 66.7% in the side span.

Given that the final failure scenario, where the bridge becomes a three-span simply supported structure, was pre-designed and calculated, the structure proves reliable due to

the effective activation of ALPs. The critical failure scenarios requiring attention are those involving the dismantling of upper chords under significant tension (steps 2, 3, 4, and 6), where the dynamic response to sudden member breakage must be carefully considered.

4.3. Dynamic Response

The focus is on the dynamic response of sudden breakages of temporary upper chords. The failure of these members within a short time frame results in a significant dynamic response in the remaining structure. To analyze the impact of temporary members on the entire structure following their removal, the failure times are set to 1 s (model 1#) and 0.01 s (model 2#) for comparative analysis. Subsequent structural response analysis steps are set to 5 s. The four temporary upper chords are designated as ①, ②, ③, and ④, corresponding to the order of their dismantling. Based on the static stress changes before and after the removal of these members and their positions, the dynamic response analysis locations for the chords are selected as shown in Figure 6.

(**a**)

(**b**)
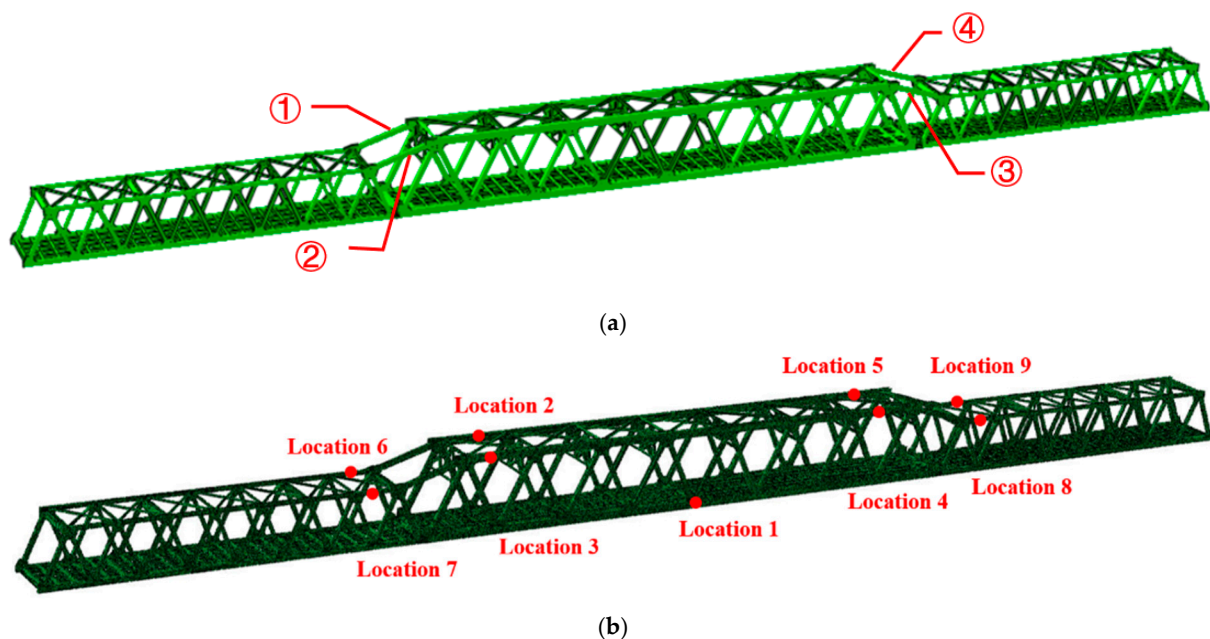
Figure 6. Schematic diagram of dynamic response analysis. (**a**) Diagram of dismantlement sequence. (**b**) Node location diagram of steel truss bridge chord.

Figure 7 presents the dynamic responses at position 1 for the two failure times, which are compared and analyzed. The initial stress value at the joint located at the mid-span position of the lower chord is 28.3 MPa for both failure times (0.01 s and 1 s). After the dismantling of rod ①, the peak stress response in Model 1# is 38.3 MPa, while in Model 2# it is 32.1 MPa, eventually stabilizing at 31.1 MPa. Following the removal of rod ②, the peak stress response in Model 1# is 41.6 MPa, compared to 37.2 MPa in Model 2#, with a stable stress value of 35.2 MPa. After the dismantling of rod ③, the peak stress response reaches 47.9 MPa in Model 1# and 43.3 MPa in Model 2#, eventually stabilizing at 41.8 MPa. After rod ④ is removed, the peak stress response is 55.1 MPa in Model 1# and 47.8 MPa in Model 2#, stabilizing at 44.7 MPa. The calculation results indicate that the stress peak at the joint is reached within 5 s of dismantling a temporary member, with stress fluctuations gradually decreasing and stabilizing, while the stable stress value increases progressively. For rods ①, ②, and ④, the nodes reached peak stress within 0.5 s, whereas for rod ③, peak stress appeared more slowly, approximately 3 s after dismantling. The model with a failure time of 0.01 s exhibits smaller differences in peak stress fluctuations compared to the 1 s failure time, with the smallest difference (10.2%) occurring after dismantling rod ③ and the largest (19.3%) after dismantling rod ①. This suggests that shorter failure times of rods

lead to more significant dynamic responses in the structure. To further assess the adverse effects of sudden member breakages on the structure, the results from the dynamic model with a 0.01 s failure time are analyzed below.
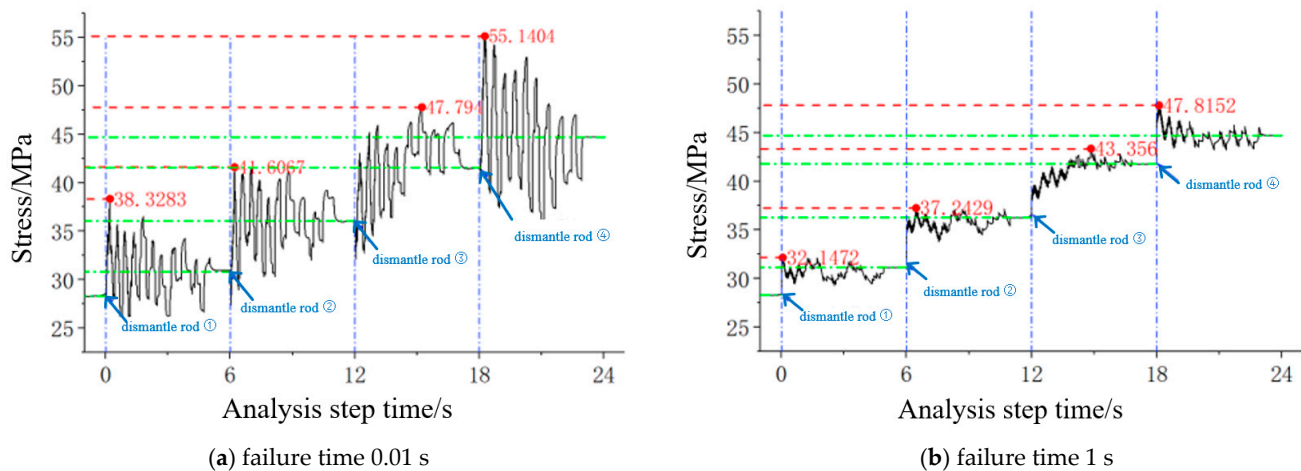

(**a**) failure time 0.01 s   (**b**) failure time 1 s

Figure 7. Comparison of stress time-history at location 1.

Figure 8 illustrates the stress time-history response of nodes positioned along the chord of the main truss during the temporary member dismantlement process. For the 128 m span, nodes at positions 2, 3, 4, and 5 of the upper chords adjacent to the removed member were selected for analysis. The figure reveals that the stress at these nodes increases from approximately 6.5 MPa to around 15 MPa following the dismantlement of the temporary member. This increase in stress is primarily observed after the failure of the adjacent temporary member. The dynamic response of the upper chord nodes to the failure of the temporary member is significant. The timing and location of the stress peak are influenced by the distance of the dismantled rod. When the node and the dismantled rod are on the same side of the truss, the stress peak occurs within 0.25 s after the rod failure. Conversely, if the dismantled rod is on the opposite side of the truss, the stress peak appears significantly later compared to the same side. For instance, when rod ② is dismantled, the stress at node position 4 peaks after 3 s. The maximum stress peak observed throughout the process occurs at position 4 following the dismantlement of rod ③. Additionally, it is evident from the figure that, after the removal of rods ① and ③, the stress at positions 3 and 5, which are not adjacent to the upper chord on the same side of the truss, exhibits considerable fluctuation without a stable trend over a short period.

For the 80 m span, nodes at positions 6, 7, 8, and 9 of the upper chords adjacent to the dismantled rod were selected for analysis. The figure indicates that the stress at these nodes decreased from approximately 50 MPa to about 20 MPa following the temporary member's failure, with the stress reduction primarily occurring due to the failure of the adjacent temporary member. The dynamic response of the chord nodes in the 80 m span to the dismantlement of the temporary member is notably pronounced, and the stress fluctuation amplitude for some nodes is greater than that observed in the 128 m span. After the dismantlement of rod ①, position 7 exhibits the largest stress fluctuation, with an amplitude reaching 60 MPa. Following the removal of rods ① and ②, the stress at positions 6 and 7 is completely released, and further dismantlement of additional rods has minimal impact. The stress response at positions 8 and 9 is more complex, with prolonged periods of significant fluctuation. Throughout the process, the maximum stress peak occurs at position 9 after the removal of rod ③. When the node and the dismantled rod are on the same side of the truss, the stress peak is reached within 0.3 s; otherwise, the peak appears noticeably later. The pattern of peak occurrence is generally consistent with that observed in the 128 m span chord.

(**a**) stress at position 2

(**b**) stress at position 3

(**c**) stress at position 4

(**d**) stress at position 5

(**e**) stress at position 6

(**f**) stress at position 7

(**g**) stress at position 8

(**h**) stress at position 9
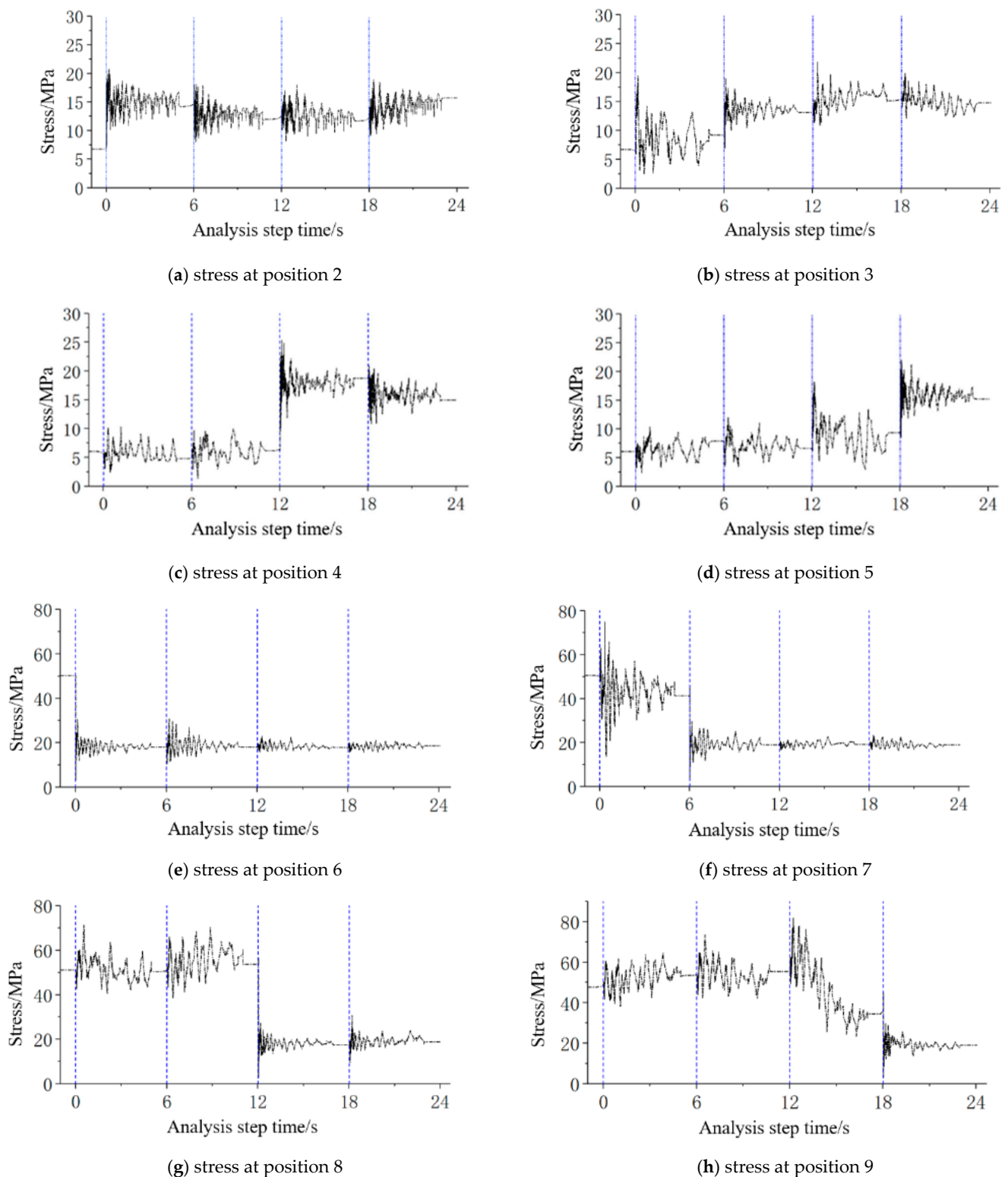
Figure 8. Stress time-history response of the upper chord on the steel truss bridge.

Figure 9 presents the stress time-history response of nodes at various positions within the main truss web during temporary member failure. The dynamic responses of four web position nodes for the 128 m span, adjacent to the temporary upper chord, are compared. Prior to the removal of the temporary members, the stress at these web position nodes is 42 MPa. This stress is alleviated by the failure of the adjacent temporary members, reducing to 29 MPa after all temporary members have been dismantled. The peak stress at the web

position adjacent to the dismantled rod is observed to develop more rapidly, with the maximum stress peak occurring at position 4 after the dismantling of rod ③, measuring 59.65 MPa.

Similarly, the dynamic responses of four web position nodes adjacent to the temporary upper chord of the 80 m span are analyzed. Initially, the stress at these web position nodes is 15 MPa before the failure of the temporary members and increases to 21.5 MPa afterward. The dynamic response of the 80 m web is more pronounced compared to the 128 m web, with the greatest impact effect observed at the web adjacent to the dismantled rod, exhibiting a maximum fluctuation amplitude of approximately 30 MPa. Additionally, the peak time of the web located on the side opposite to the dismantled rod occurs significantly later than that of the web on the same side. The stress fluctuation amplitude for the web on the opposite side is within 10 MPa, indicating less pronounced stress changes.
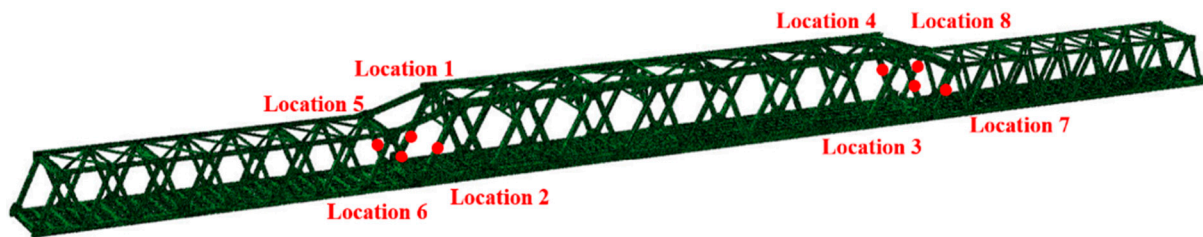
(**1**) Node location diagram of steel truss bridge web rod
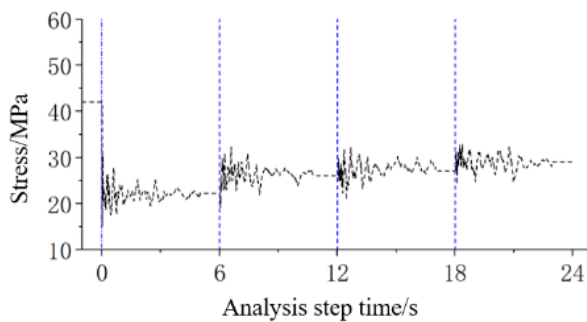
(**a**) stress at position 1
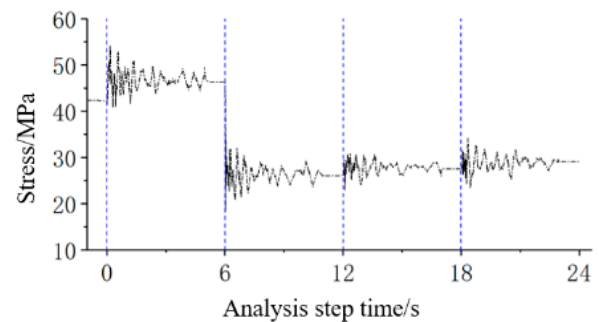
(**b**) stress at position 2
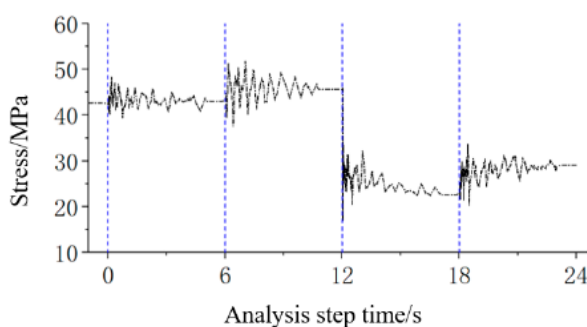
(**c**) stress at position 3
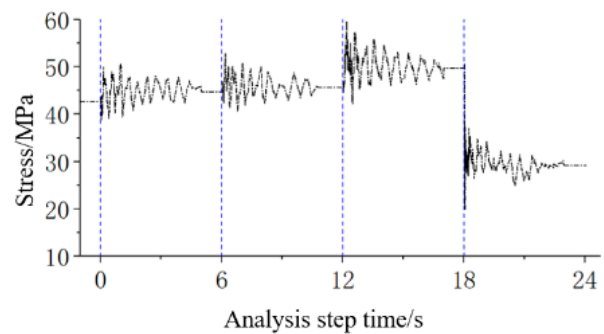
(**d**) stress at position 4

Figure 9. *Cont.*

(**e**) stress at position 5

(**f**) stress at position 6

(**g**) stress at position 7

(**h**) stress at position 8
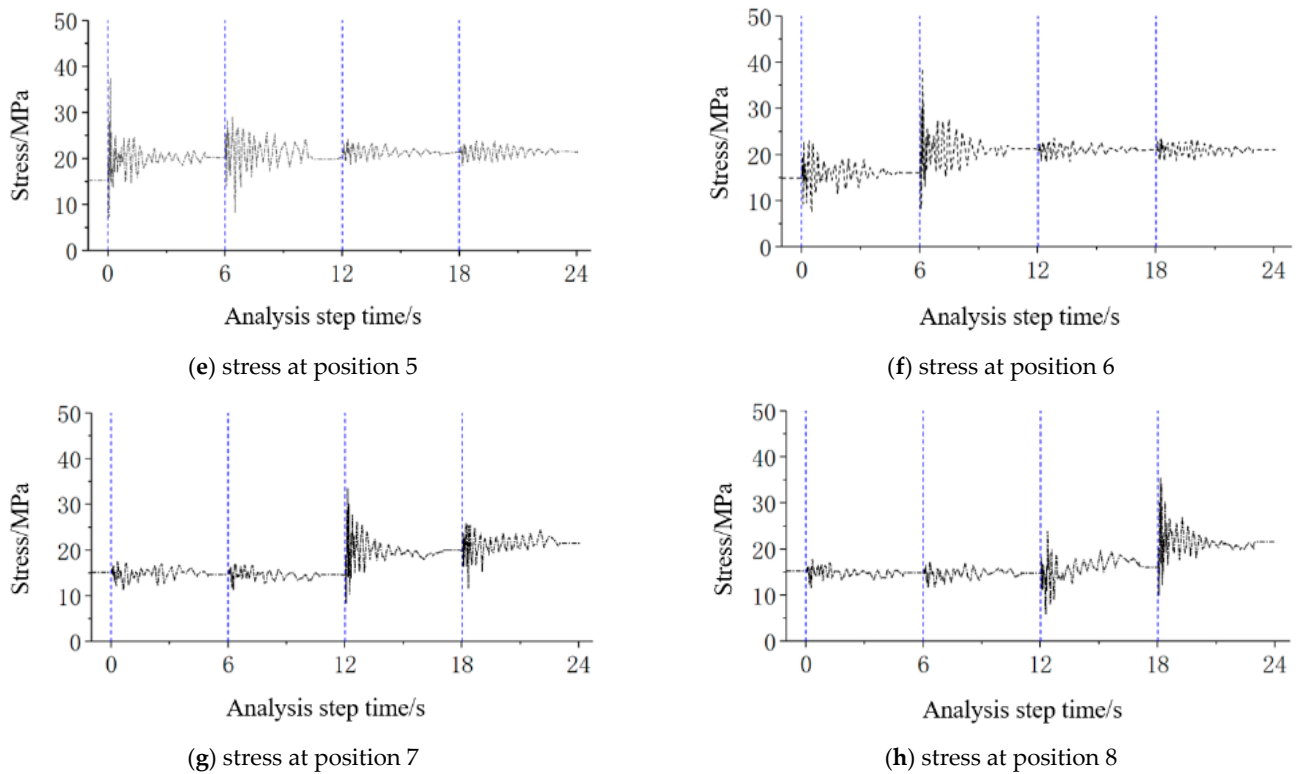
Figure 9. Stress time-history response of the web rod on the steel truss bridge.

The main structural components are made of Q370 steel, which has an allowable stress value of 220 MPa. During the construction process, this allowable stress can be increased by 1.2 times under dead load and construction load conditions, resulting in a maximum allowable stress of 264 MPa. Figure 10 displays the maximum stress values observed in the structure following the dismantling of rods ①, ②, ③, and ④. According to the calculation results, the maximum stress values after dismantling each rod are as follows: 232 MPa for rod ①, 217.6 MPa for rod ②, 237.1 MPa for rod ③, and 200.1 MPa for rod ④. These values, while all below the allowable stress limit of 264 MPa, are close to this threshold. The maximum stress peaks occur within 1 s after the failure of the temporary members. Notably, the dynamic stress generated by the removal of rods ① and ③ is greater than that resulting from the removal of rods ② and ④.

Figure 10. Maximum stress time-history diagram of the steel truss bridge structure.

5. Robustness-Enhanced Method and Tests

Given that the maximum stress response of the structure is close to the allowable value, this section presents a structural retrofitting method for robustness enhancement. A relevant simulation test was conducted to evaluate the effectiveness of this robustness-enhancement method, which was subsequently applied in failure scenarios equipped with a comprehensive monitoring system.

5.1. Structural Retrofitting Method for Robustness Enhancement

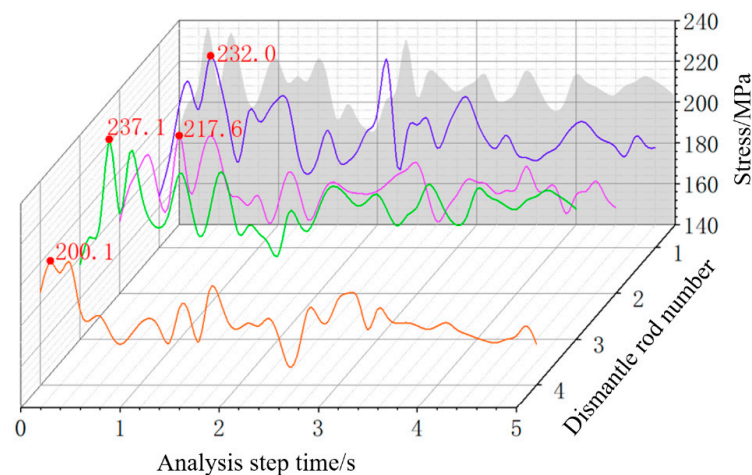The study of the structural retrofitting method for robustness enhancement can be a challenging task due to the particularity of different configuration of the structure, nature of the triggering event and size of the initial failure [10]. The strengthening and retrofitting techniques can be categorized on the three criteria definitions: (i) preventing initial failure, (ii) controlling collapse propagation, and (iii) controlling the final collapse status [30]. The majority of strengthening techniques focus on redistribution-type collapses, in which alternate load paths (ALPs) have a determining role. Therefore, measures that try to increase the structural robustness by adding new load paths (or strengthening the existing ones), namely, improving catenary behavior in beams or cable strengthening of beams, adding trusses, or enhancing connections [31], are usually useful mainly in the case of redistribution-type collapses [32]. For other scenarios, i.e., impact-type collapses, the effectiveness of these techniques is under question and other techniques, namely, energy absorber devices [33], should be utilized instead [30,34].

In the failure scenario of this steel truss bridge, the members' fracture location, i.e., the initial failure, is determined, so preventing the initial failure is more economical and effective. Considering that the dynamic response mainly comes from the initial tension of the broken members, the fluctuation amplitude of which is up to 60 MPa, based on the idea of reducing the initial tension to prevent the initial failure, a structural retrofitting method of jacking a truss girder above the side pier to reduce the tension of the temporary upper chord above the middle pier was proposed. The application of bridge jacking technology in bridge retrofitting has gradually developed into a promising mature practical technology [35]. The internal force distribution of the steel truss can be changed through jacking technology [36], but the specific applied method and effect need to be verified [37–39].

5.2. Simulated Jacking Experimental Test

The relationship between the jacking height and the internal force of the temporary upper chord requires verification. For this purpose, a simulated jacking experiment was conducted under the working condition of the steel truss girder reaching pier 14#. The boundary conditions of the 80 m span in this experiment were maintained consistent with those prior to the system transformation. During the simulated jacking experiment, the front end of the truss girder above pier 14# was jacked, and both the jacking height and the stress in the temporary members above the adjacent pier 13# were monitored. The goal of this simulated jacking experiment was to gather relevant data to support the subsequent dismantlement of temporary members and to assess the feasibility of the robustness-enhancement method.

In the simulated jacking experiment, five working conditions were examined: before lifting, lifting by 46 mm, lifting by 96 mm, lifting by 122.8 mm, and restoring to the original height. The calculation results indicate that the upper chord transitions from tension to compression under the condition of lifting by 122.8 mm. Measurement points were defined as follows: point 7-1 represents the upper edge of the temporary upper chord, point 7-2 represents the lower edge of the temporary upper chord, point 19-1 represents the upper edge of the temporary lower chord, and point 19-2 represents the lower edge of the temporary lower chord.

Figure 11 illustrates the relationship between the jacking height and the stress in the temporary members. The test results indicate that as the jacking height increases, the stress in the temporary upper chord decreases, while the stress in the temporary lower

chord gradually increases. Specifically, when the jacking height reaches 122.8 mm, the stress at the upper edge of the upper chord shifts from 9.6 MPa to −32.2 MPa, and the stress at the lower edge of the upper chord changes from 29.2 MPa to 10.3 MPa. After completing the jacking operation and restoring the front end of the steel truss girder to its original height, the internal forces in the members return to levels comparable to the initial state. The monitoring results from the simulated jacking experiment are consistent with the calculation results, confirming that the structural retrofitting method involving jacking effectively reduces the internal force in the upper chord.
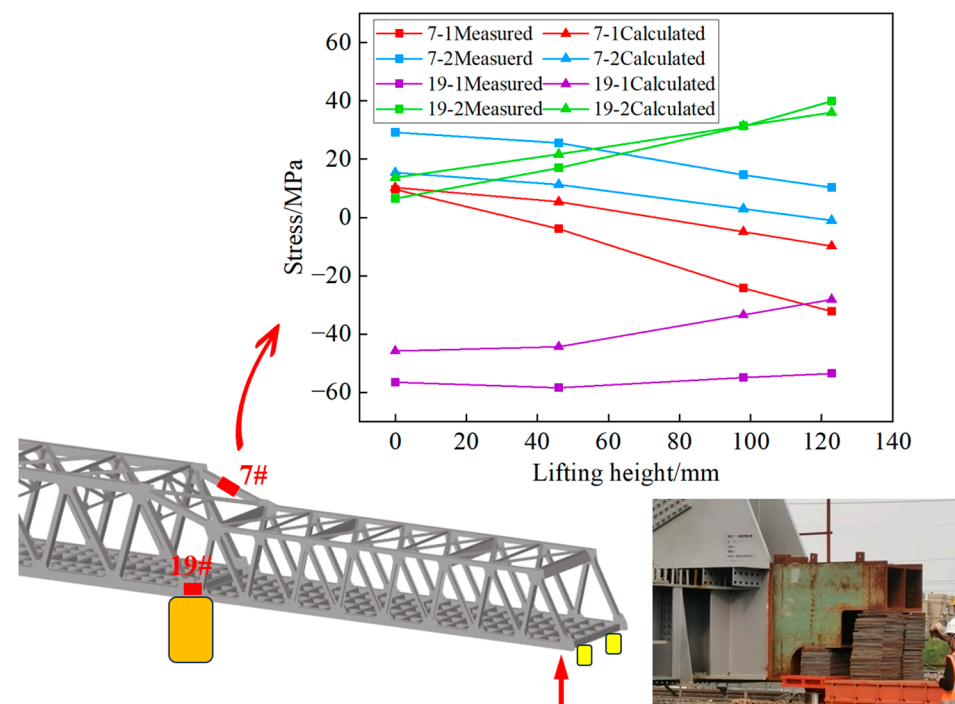

Figure 11. Relationship between jacking height and stress of temporary members.

5.3. Formal Jacking Experimental Test

The effectiveness of the robustness-enhanced method was verified by simulated jacking experiments. The sequence for dismantling the temporary members was determined as follows: First, the truss girder above pier 16# was lifted, and the temporary members above pier 15# (north side) were dismantled. Next, the truss girder above pier 13# was lifted, and the temporary members above pier 14# (south side) were dismantled. The specific steps for dismantling temporary members on one side are outlined below, as shown in Figure 12:

Step 1: Monitor the stress of the temporary members, and then use the 80 m span end lifting jack and pads to adjust the elevation, aiming to bring the temporary members close to a stress-free state;

Step 2: Cut temporary short flat joint welded joints, and then remove high-strength bolts connected with long flat joints;

Step 3: Weld and remove the lifting lugs on the temporary rods, cut the chords in sections avoiding the transverse partition, and remove the temporary upper chords on the west side first by using the crawler crane;

Step 4: Remove the temporary lower chord on the east side;

Step 5: Use flame cutting to remove the temporary connection of the lower chord, and grind the area to restore the original shape of the steel truss beam.

Step 6: Complete the dismantlement work and return the structure to the original height.
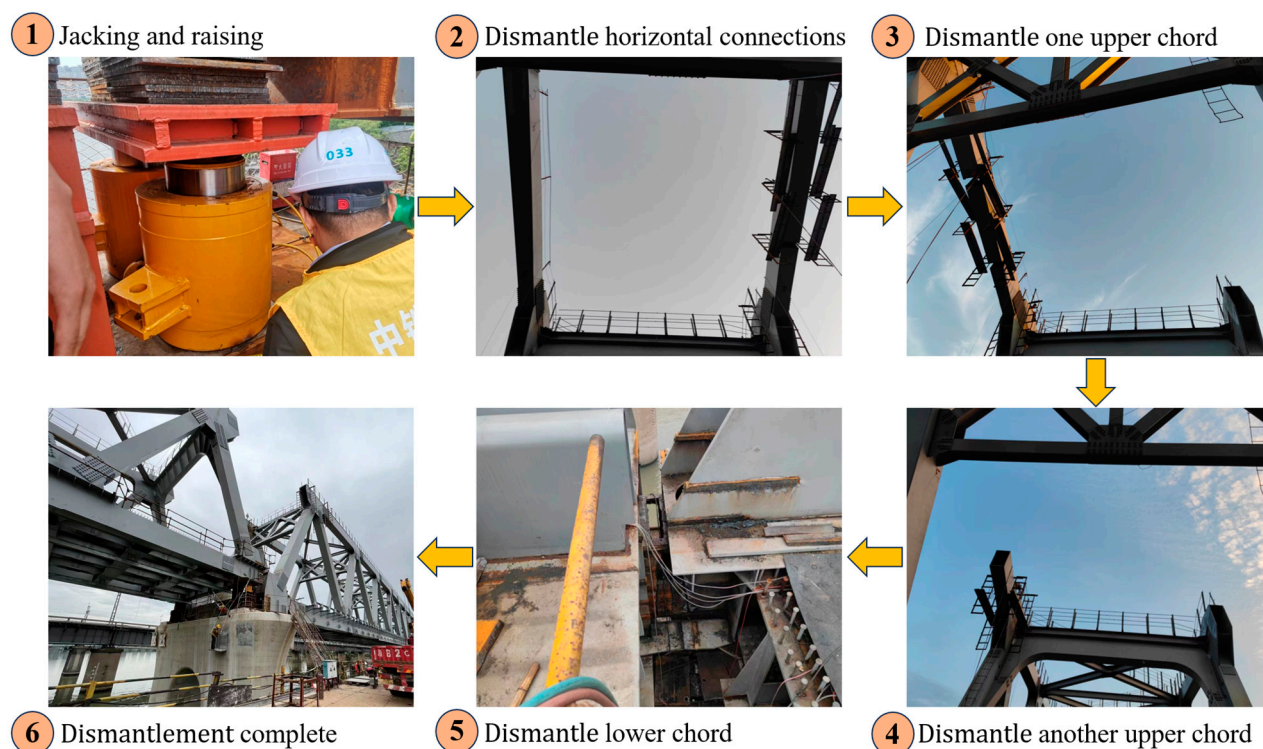
Figure 12. Dismantlement process.

In the formal test, the jacking height of the truss girder above pier 16# was set to 46 cm. Stress measurements of the temporary members on both the east and west sides of the truss above pier 15# were recorded. The monitoring results are presented in Table 2. The initial combined stress reflects the actual stress resulting from the combined effects of bending moments, axial forces, and other factors; the axial stress calculation is based on the average stress values at both the upper and lower edges of the member. Following the jacking operation, the internal forces in the temporary upper chords on both the east and west sides shifted from tension to compression. While the stress in the temporary lower chords increased, they remained in a compressed state.

Table 2. Monitoring results of temporary members in the final test. Units: MPa.

Position	Section	Initial Combined Stress	Initial Axial Stress	Combined Stress after Jacking	Axial Stress after Jacking
East	7-1	127.3	88.9	−43.9	−29.8
	7-2	50.5		−15.8	
	19-1	17.2	−53.8	−59.3	−27.6
	19-2	−124.8		4.1	
West	7-1	164.1	101.8	−20.3	−25.5
	7-2	39.4		−30.8	
	19-1	60.4	−48.1	−17.3	−3.2
	19-2	−156.6		10.9	

In the final dismantlement state, the internal forces of temporary upper and lower chords are pressure forces, so there will be no extra dynamic response during dismantlement. Changes in the internal forces of adjacent rods during the dismantlement process should be monitored [36]. Initially, the temporary horizontal connections had been removed. The dismantlement process began with the temporary upper chord on the west side, followed by the temporary upper chord on the east side. Monitoring was conducted

on the upper chord (4#), webs (5#), and lower chord (6#) on both the east and west sides adjacent to the dismantled members.

Figure 13 displays the stress monitoring results for the adjacent members during the dismantlement process. Generally, the stress in most adjacent members decreased. Due to the differing dismantlement sequences of the temporary upper chords on the east and west sides, stress changes in adjacent members varied between the two sides at different stages of dismantlement. However, once both temporary upper chords were fully dismantled, the stress change values for the adjacent upper and lower chords on both sides were similar. Specifically, the stress in the upper chords decreased by 36.9 MPa on the east side and 32.9 MPa on the west side, while the stress in the lower chords decreased by 25.9 MPa on the east side and 18.3 MPa on the west side.
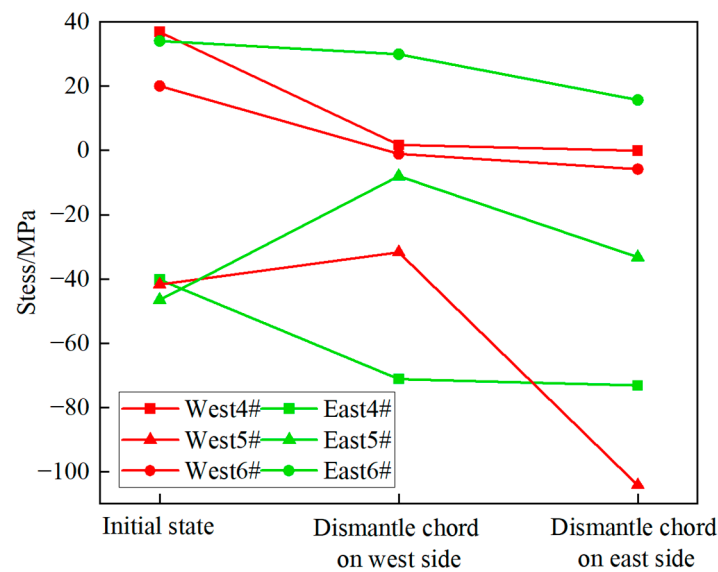

Figure 13. Stress monitoring results of adjacent members during temporary members' dismantlement.

6. Conclusions

This paper presents a unique case study of a steel truss bridge under construction that experienced sudden member failures. These failures occurred due to dismantlement during an unconventional continuous-to-simply-supported incremental launching process, and were monitored extensively using a comprehensive monitoring system. The robustness of the structure was evaluated through computer simulations of various failure scenarios to analyze the bridge's capacity to effectively activate alternative load paths. Additionally, both simulated and formal experimental tests were conducted to verify the effectiveness of the proposed robustness-enhancement method. The study's conclusions are as follows:

1. During the analysis of robustness in temporary member failure scenarios determined by the dismantlement sequence, it was found that

    -   The stresses on the upper chords adjacent to the dismantled rod experienced the highest increase of up to 270%.
    -   The maximum deflection increased by up to 19.0% at the middle span and 66.7% at the side span.
    -   The structural bridge had structural redundancy based on the effective activation of ALPs.

2. The dynamic response primarily stemmed from the initial tension in the temporary upper chords, with fluctuation amplitudes reaching up to 60 MPa. The shorter the failure time of the rods, the more pronounced the dynamic response of the structure.

3. A structural retrofitting method involving jacking the truss girder above the side pier to reduce the tension in the temporary upper chord above the middle pier was

proposed. The effectiveness of this method was demonstrated through both simulated experimental tests and formal experimental tests.

4. The proposed unconventional continuous-to-simply-supported incremental launching method for a steel truss bridge has been proven to be safe and feasible. However, dismantling members with significant initial tension requires careful attention during the system transformation process. The proposed structural retrofitting method, which aims to enhance robustness, effectively reduces the initial tension in members, thereby preventing initial failure. Based on the findings of this study, future research could explore potential improvements and new approaches in the study of steel truss bridge robustness, particularly in preventing initial failure.

Author Contributions: Y.C. (Yanming Chen): Conceptualization, Methodology, Writing—review & editing. Y.L.: Project administration, Resources. L.Z.: Supervision, Resources, Writing—review & editing. L.C.: Supervision, Resources, Validation. Y.C. (Yilian Chen): Data curation, Writing—review & editing. All authors have read and agreed to the published version of the manuscript.

Data Availability Statement: The original contributions presented in the study are included in the article, further inquiries can be directed to the corresponding authors.

Conflicts of Interest: Author Yong Liao was employed by the company China Railway No. 2 Engineering Group Co., Ltd. The remaining authors declare that the research was conducted in the absence of any commercial or financial relationships that could be construed as a potential conflict of interest.

References

1. Chen, X.; Li, H.; Agrawal, A.K.; Ettouney, M.; Wang, H. Alternate load paths redundancy analysis of steel truss bridges. *J. Bridge Eng.* **2022**, *27*, 04022106. [CrossRef]
2. Okur, E.K.; Okur, F.Y.; Altunişik, A.C.; Günaydin, M.; Adanur, S. Progressive collapse assessment of Osmangazi Suspension Bridge due to sudden hanger breakage under different loading conditions. *Eng. Fail. Anal.* **2023**, *149*, 107269. [CrossRef]
3. López, S.; Makoond, N.; Sánchez-Rodríguez, A.; Adam, J.M.; Riveiro, B. Learning from failure propagation in steel truss bridges. *Eng. Fail. Anal.* **2023**, *152*, 107488. [CrossRef]
4. Stark, T.D.; Benekohal, R.; Fahnestock, L.A.; LaFave, J.M.; He, J.; Wittenkeller, C. I-5 Skagit river bridge collapse review. *J. Perform. Constr. Facil.* **2016**, *30*, 04016061. [CrossRef]
5. Birajdar, H.S.; Maiti, P.R.; Singh, P.K. Failure of Chauras bridge. *Eng. Fail. Anal.* **2014**, *45*, 339–346. [CrossRef]
6. Deng, L.; Wang, W.; Yu, Y. State-of-the-art review on the causes and mechanisms of bridge collapse. *J. Perform. Constr. Facil.* **2016**, *30*, 04015005. [CrossRef]
7. Wardhana, K.; Hadipriono, F.C. Analysis of recent bridge failures in the United States. *J. Perform. Constr. Facil.* **2003**, *17*, 144–150. [CrossRef]
8. Simoncelli, M.; Aloisio, A.; Zucca, M.; Venturi, G.; Alaggio, R. Intensity and location of corrosion on the reliability of a steel bridge. *J. Constr. Steel Res.* **2023**, *206*, 107937. [CrossRef]
9. Zhang, G.; Liu, Y.; Liu, J.; Lan, S.; Yang, J. Causes and statistical characteristics of bridge failures: A review. *J. Traffic Transp. Eng. (Engl. Ed.)* **2022**, *9*, 388–406. [CrossRef]
10. Kiakojouri, F.; Sheidaii, M.R.; De Biagi, V.; Chiaia, B. Progressive collapse of structures: A discussion on annotated nomenclature. *Structures* **2021**, *29*, 1417–1423. [CrossRef]
11. Torres, B.; Poveda, P.; Ivorra, S.; Estevan, L. Long-term static and dynamic monitoring to failure scenarios assessment in steel truss railway bridges: A case study. *Eng. Fail. Anal.* **2023**, *152*, 107435. [CrossRef]
12. Derseh, S.A.; Mohammed, T.A. Bridge structures under progressive collapse: A comprehensive state-of-the art-review. *Results Eng.* **2023**, *18*, 101090. [CrossRef]
13. Caredda, G.; Makoond, N.; Buitrago, M.; Sagaseta, J.; Chryssanthopoulos, M.; Adam, J.M. Learning from the progressive collapse of buildings. *Dev. Built Environ.* **2023**, *15*, 100194. [CrossRef]
14. Makoond, N.; Shahnazi, G.; Buitrago, M.; Adam, J.M. Corner-column failure scenarios in building structures: Current knowledge and future prospects. *Structures* **2023**, *49*, 958–982. [CrossRef]
15. Russell, J.M.; Sagaseta, J.; Cormie, D.; Jones, A. Historical review of prescriptive design rules for robustness after the collapse of Ronan Point. *Structures* **2019**, *20*, 365–373. [CrossRef]

16. Adam, J.M.; Parisi, F.; Sagaseta, J.; Lu, X. Research and practice on progressive collapse and robustness of building structures in the 21st century. *Eng. Struct.* **2018**, *173*, 122–149. [CrossRef]

17. Vanova, P.; Sun, Z.; Odinson, O.; Jiang, Z. Dynamic response analysis of a model truss bridge considering damage scenarios. *Eng. Fail. Anal.* **2023**, *151*, 107389. [CrossRef]

18. Buitrago, M.; Makoond, N.; Moragues, J.J.; Sagaseta, J.; Adam, J.M. Robustness of a full-scale precast building structure subjected to corner-column failure. *Structures* **2023**, *52*, 824–841. [CrossRef]

19. Padil, K.H.; Bakhary, N.; Abdulkareem, M.; Li, J.; Hao, H. Non-probabilistic method to consider uncertainties in frequency response function for vibration-based damage detection using Artificial Neural Network. *J. Sound Vib.* **2020**, *467*, 115069. [CrossRef]

20. Teng, S.; Chen, X.; Chen, G.; Cheng, L. Structural damage detection based on transfer learning strategy using digital twins of bridges. *Mech. Syst. Signal Process.* **2023**, *191*, 110160. [CrossRef]

21. Buitrago, M.; Bertolesi, E.; Calderón, P.A.; Adam, J.M. Robustness of steel truss bridges: Laboratory testing of a full-scale 21-metre bridge span. *Structures* **2021**, *29*, 691–700. [CrossRef]

22. Bertolesi, E.; Buitrago, M.; Adam, J.M.; Calderón, P.A. Fatigue assessment of steel riveted railway bridges: Full-scale tests and analytical approach. *J. Constr. Steel Res.* **2021**, *182*, 106664. [CrossRef]

23. Caredda, G.; Porcu, M.C.; Buitrago, M.; Bertolesi, E.; Adam, J.M. Analysing local failure scenarios to assess the robustness of steel truss-type bridges. *Eng. Struct.* **2022**, *262*, 114341. [CrossRef]

24. Sun, Y.; Tai, X.; Liu, K.; Zhu, A.; Zhu, H. Determining launching construction parameters of superlong superwide bridges: A multiobjective optimization method using machine learning techniques. *Structures* **2022**, *41*, 15–28. [CrossRef]

25. Yu, X.; Deng, Y.; Yan, B. Case study of the 156 m simply supported steel truss railway bridge. *Struct. Eng. Int.* **2017**, *27*, 563–568. [CrossRef]

26. Wu, X.; Wu, T.; Chen, W. Analysis of height difference between three trusses of a steel truss bridge during incremental launching. *Stahlbau* **2018**, *87*, 910–922. [CrossRef]

27. Wu, G.; Qiu, W.; Wu, T. Nonlinear dynamic analysis of the self-anchored suspension bridge subjected to sudden breakage of a hanger. *Eng. Fail. Anal.* **2019**, *97*, 701–717. [CrossRef]

28. Soto, N.; Cid, C.; Baldomir, A.; Hernández, S. Fail-safe optimum cable system under cable breakage in cable-stayed bridges. Application to the Queensferry Crossing Bridge. *Eng. Struct.* **2023**, *279*, 115557. [CrossRef]

29. Ruiz-Teran, A.; Aparicio, A. Response of under-deck cable-stayed bridges to the accidental breakage of stay cables. *Eng. Struct.* **2009**, *31*, 1425–1434. [CrossRef]

30. Kiakojouri, F.; De Biagi, V.; Chiaia, B.; Sheidaii, M.R. Strengthening and retrofitting techniques to mitigate progressive collapse: A critical review and future research agenda. *Eng. Struct.* **2022**, *262*. [CrossRef]

31. Wang, J.; Ke, K.; Yam, M.C.; Teng, M.; Wang, W. Improving structural robustness of steel frame buildings by enhancing floor deck connections. *J. Constr. Steel Res.* **2023**, *204*, 107842. [CrossRef]

32. Anitori, G.; Casas, J.R.; Ghosn, M. Redundancy and robustness in the design and evaluation of bridges: European and North American perspectives. *J. Bridge Eng.* **2013**, *18*, 1241–1251. [CrossRef]

33. Li, Y.; Li, S.; Tan, P. A novel tuned mass damper inerter: Optimal design, effectiveness comparison, and robustness investigation. *Structures* **2023**, *55*, 1262–1276. [CrossRef]

34. Kiakojouri, F.; De Biagi, V.; Chiaia, B.; Sheidaii, M.R. Progressive collapse of framed building structures: Current knowledge and future prospects. *Eng. Struct.* **2020**, *206*, 110061. [CrossRef]

35. Gao, H.; Li, B.; Jian, J.; Yu, T.; Liu, H. Integral jacking of concrete continuous box beam bridge. *Structures* **2023**, *54*, 1026–1045. [CrossRef]

36. Wang, Y.; Thrall, A.P.; Zoli, T.P. Behavior of the Delaware River Bridge during repair. *J. Constr. Steel Res.* **2021**, *177*, 106448. [CrossRef]

37. Xiao, F.; Hulsey, J.L.; Chen, G.S.; Xiang, Y. Optimal static strain sensor placement for truss bridges. *Int. J. Distrib. Sens. Netw.* **2017**, *13*, 1550147717707929. [CrossRef]

38. Xu, C.; Guo, C.; Xu, Q.; Yang, Z. The global collapse resistance capacity of a seismic-damaged SRC frame strengthened with an enveloped steel jacket. *Structures* **2021**, *33*, 3433–3442. [CrossRef]

39. Xiao, F.; Hulsey, J.L.; Balasubramanianm, R. Fiber optic health monitoring and temperature behavior of bridge in cold region. *Struct. Control. Health Monit.* **2017**, *24*, e2020. [CrossRef]